ACS Catalysis

pubs.acs.org/acscatalysis
Research Article

Solvent-Free Benzyl Alcohol Oxidation Using Spatially Separated Carbon-Supported Au and Pd Nanoparticles

Xiaoliang Li, Liang Zhao, Mark Douthwaite,* Kai Wang, Ouardia Akdim, Isaac T. Daniel, Rena Oh, Lei Liu, Zhe Wang, Fanhui Meng, Samuel Pattisson, Angeles López-Martin, Jian Yang, Xiaoyang Jerry Huang,* Richard J. Lewis, and Graham J. Hutchings*

Cite This: ACS Catal. 2024, 14, 16551−16561
Read Online

ACCESS | Metrics & More | Article Recommendations | Supporting Information

ABSTRACT: The spatial separation of Au and Pd nanoparticles supported on carbon has been demonstrated to be highly effective in facilitating aqueous-phase alcohol oxidation reactions, wherein OH^- is the oxidant terminal for the oxidative dehydrogenation reaction. However, the application of this methodology in nonaqueous environments has not yet been explored. Supported alloyed Au−Pd nanoparticles are known to be highly active in the solvent-free oxidation of benzyl alcohol with oxygen as the terminal oxidant, leading to benzaldehyde by direct oxidation and toluene by disproportionation. Here, we show that by physically separating Au and Pd nanoparticles supported on carbon, the reaction rate for solvent-free benzyl alcohol oxidation can be further enhanced by coupling the oxidation and disproportionation reactions via H-transfer from Pd to Au.

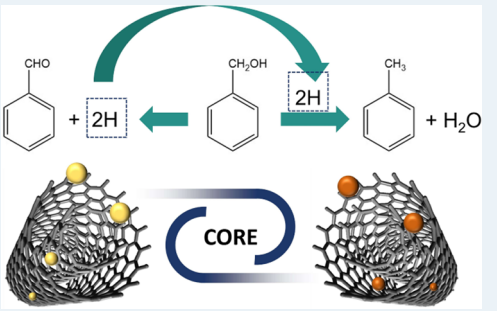

KEYWORDS: *Au−Pd separation, carbon nanotubes, solvent-free alcohol oxidation, coupling effect, H-transfer, cooperative redox enhancement*

INTRODUCTION

The cooperative redox enhancement (CORE) effect describes the catalytic enhancement observed when two spatially separated metals supported on a conducting support are combined to catalyze redox reactions. We have previously shown that the CORE effect operates in a similar manner to an electrochemical fuel cell, where each component metal catalyzes one of the individual half-reactions that make up the full redox process.[1] We demonstrated that in aerobic alcohol oxidation over Au and Pd, each metal can separately catalyze the two crucial mechanistic steps, i.e., oxidative dehydrogenation (ODH) and oxygen reduction (ORR). The properties of the support material are considered to be critically important in facilitating the CORE effect, providing a pathway for electrons to be shuttled between the metal active sites. We have since observed that the physicochemical properties and molar ratio of the two (coupled) metals can also have a significant impact on the magnitude of the CORE effect.[2]

Recently, we established that the origin of this enhancement is derived from the electrochemical polarization of component metal sites. This, in essence, reduces the activation barriers for each half-reaction, enabling the primary ODH transformation to proceed at a significantly enhanced rate. We also demonstrated that these effects are not strictly limited to Au and Pd, and through combined electrochemical and thermochemical testing, we have been able to provide a clear set of conditions that need to be met to observe the CORE effect in a given reaction.[1−5] The discovery of this novel effect will provide the scientific community with a completely new avenue for catalyst and process design. There are several reports in which researchers have suggested that component ODH and ORR half-reactions can be catalyzed independently over monometallic Au and Pt catalysts.[6,7] Furthermore, more recently, it has been demonstrated that hydrogen oxidation and nitrophenol reduction can also be electrochemically coupled but in a thermochemical setting.[8] Collectively, these studies demonstrate that the CORE effect is likely to be an extremely general phenomenon that, if harnessed effectively, could have a significant impact on catalysis science moving forward.

One feature that, until now, has appeared to be necessary to facilitate CORE is the presence of an electrolyte. In previous examples, we used $NaHCO_3$ (0.4 M) and typically operated our thermocatalytic reactions at pH = 8.7. In the CORE mechanism, the electrolytes and collision among catalytic grains enable the transfer of charges within the system. This movement of ions maintains electrical neutrality in the solution and completes the circuit for electron flow between the metals.

Received: August 20, 2024
Revised: October 15, 2024
Accepted: October 15, 2024

https://doi.org/10.1021/acscatal.4c05019
ACS Catal. 2024, 14, 16551−16561

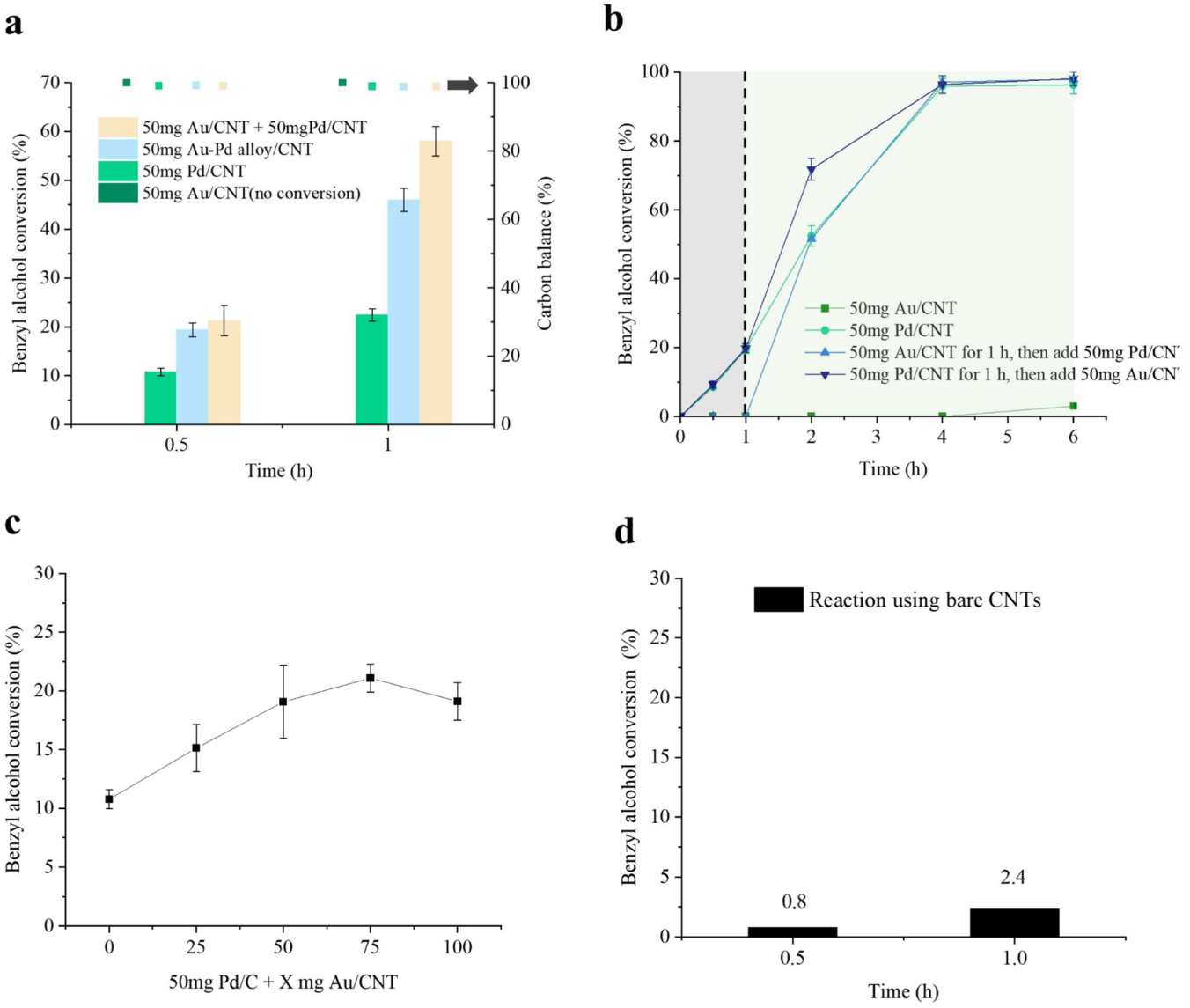

Figure 1. Solvent-free BA oxidation using Au- and Pd-based catalysts. (a) Catalytic performance of monometallic Au and Pd catalysts with corresponding alloyed and physical mixture catalysts (dots represent carbon balance). (b) Reaction with monometallic Au or Pd catalyst for 1 h by the addition of the counterpart catalyst. *Reaction conditions*: 15 mL BA, 120 °C, and 3 bar O_2; all Au and Pd weights are kept the same in each of the reactions. The associated error bars correspond to mean ± standard deviation (n = 3). (c) The addition of increasing amounts of Au/CNT (X = 0, 25, 50, 75, and 100) to the physical mixture catalysts of Au/CNT + Pd/CNT for their performance on BA conversion; reaction time: 0.5 h. (d) Reaction performance of benzyl alcohol oxidation by using the bare CNTs as a blank reaction. The only observed product is BZALD. Reaction conditions: 15 mL benzyl alcohol, 120 °C, 3 bar O_2, and reaction time: 0.5 and 1 h.

We consider that this proceeds via a Grotthuss-type mechanism and thus the independent rates of the two half-reactions are not limited by ionic charge transfer.[9] To support this hypothesis, we aim to investigate whether CORE effects can be observed in nonaqueous media, which may still accommodate this chemistry. As the solvent-free aerobic oxidation of benzyl alcohol (BA) can be catalyzed by carbon-supported Au−Pd alloy nanoparticles, we consider this reaction to be an ideal probe for this investigation.[10]

The use of supported noble metal materials as catalysts for the solvent-free oxidation of BA is a well-established area of research.[11,12] The reaction network is relatively complex (Scheme S1) but has been considered by many researchers as an ideal model reaction to study selective redox catalysis.[10,13] In the presence of a catalyst, BA can be converted to products through two competitive pathways: either through direct ODH, which leads to the formation of benzaldehyde (BZALD), or through a disproportionation reaction, in which the two molecules of BA react to form stoichiometric quantities of BZALD and toluene (TOL). Under aerobic conditions, it is widely agreed that these transformations are nonradical processes.[14,15] In contrast, the sequential oxidation of BZALD to benzoic acid (BZA) is considered to be a radical process. As such, only small quantities of BZA are observed when unreacted BA is still present in the reaction mixture as it can serve as an effective radical scavenger.[15]

Given that selective ODH of alcohols underpins many important transformations in several sectors, significant emphasis has been placed on the development of catalysts, which can effectively catalyze BA ODH and, in doing so, suppress the nondesired disproportionation reaction.[16] One

https://doi.org/10.1021/acscatal.4c05019
ACS Catal. 2024, 14, 16551−16561

particularly effective method of doing this is to employ a basic support for metal nanoparticles, such as MgO or ZnO.[17] These approaches are very effective, with extremely high BZALD selectivities often reported (>95%), albeit at a relatively lower rate of BA conversion compared to carbon-supported nanoparticle catalysts.[16,18]

Herein, using the aerobic solvent-free oxidation of BA as our model reaction, we assess the extension of the CORE effect to nonaqueous media and, in so doing, aim to gain a deeper insight into the role of the electrolyte in the CORE mechanism. For continuity, we used model catalysts similar to those adopted in our initial studies, which are comprised of monometallic and bimetallic catalysts containing Au and Pd.[1,2]

RESULTS AND DISCUSSION

Catalyst Synthesis and Characterization. Monometallic Au and Pd (0.5 wt %, respectively) and analogous Au−Pd (1.0 wt %) bimetallic alloy catalysts supported on carbon nanotubes (CNTs, inner diameter 4−8 nm and outer diameter 10−20 nm) were prepared by the sol-immobilization method.[19] The textural properties of the catalysts (Table S1) demonstrate that the immobilization of the metal species onto the CNTs has very little impact on the N_2 sorption isotherms (Figure S1). In addition, the BET surface areas (~300 $m^2\ g^{-1}$), mean pore volumes (~1.3 $cm^3\ g^{-1}$), and mean pore sizes (~17.3 nm) of the fresh supported metal catalysts are all comparable to those of the bare CNT material.

The X-ray photoelectron spectroscopy (XPS) Au 4f and Pd 3d spectra of the materials are shown in Figure S2a−f. The binding energies (BEs) of the Au $4f_{5/2}$ (~87.7 eV) and Au $4f_{7/2}$ (~84 eV) peaks exhibited by the Au/CNT before and after the reaction (Figure S2a,c) and Au−Pd/CNT alloy catalysts (Figure S2e) are indicative of metallic Au.[1,3] In contrast, the Pd 3d region of the XPS spectra indicates that both Pd/CNT and Au−Pd/CNT catalysts exhibit a proportion of Pd^{2+}, especially for the postreaction sample of Pd/CNT from its physical mixture with Au/CNT. The Pd surface is largely oxidized. Through the deconvolution of the Pd^{2+} (~336.9 eV) and Pd^0 (~335.2 eV) components, the proportion of each species among the three catalysts was determined (Table S2). Notably, a downfield shift in BE is observed in the Pd $3d_{5/2}$ region of the as-prepared Au−Pd/CNT and a postreaction sample of the Au/CNT + Pd/CNT physical mixture in their XPS spectrum, which could be a characteristic of Au and Pd interactions.[19] Further evidence of Au−Pd alloying in the as-prepared Au−Pd/CNT catalyst was acquired from energy-dispersive X-ray (EDX) analysis of scanning transmission electron microscopy (STEM) micrographs of the Au−Pd/CNT material (Figure S3). High-angle annular dark-field (HAADF) STEM images of the Au−Pd/CNT material (Figure S3) identified a mean (and narrow) particle size distribution (PSD) of 3.0 nm (standard deviation, SD = 0.7), which is slightly lower than that of the PSD of the analogous Au/CNT and Pd/CNT materials, 3.7 nm (SD = 0.7) and 3.6 nm (SD = 0.8), respectively (Figure S4).

Solvent-Free Benzyl Alcohol Oxidation. The prepared materials were employed for the aerobic solvent-free oxidation of BA. Each catalyst was used independently, and its performance was compared with that of a physical mixture of Au/CNT and Pd/CNT (denoted as Au/CNT + Pd/CNT). Note that the total amount of Au and Pd used in each reaction was consistent: 2.54×10^{-6} and 4.70×10^{-6} mol, respectively; and the total weight loading (1.0 wt %) of Au and Pd was kept constant for each experiment. The monometallic Au/CNT catalyst exhibited no activity over reaction durations of 0.5 and 1 h (Figure 1a). Nevertheless, the BA conversion over a physical mixture of the two monometallic catalysts (57.5% at 1 h) was far greater than the sum of the conversions of the monometallic Au/CNT and Pd/CNT catalysts (46% at 1 h), indicating that there is a clear enhancement effect between the physically mixed monometallic Au/CNT and Pd/CNT catalysts. Strikingly, the rate of BA conversion in the presence of the Au/CNT and Pd/CNT physical mixture (k = 1.55 $mM\cdot s^{-1}$) was greater than that observed over the Au−Pd/CNT alloy (k = 1.23 $mM\cdot s^{-1}$), which was prepared by the same method, emphasizing again the significant effect when Au and Pd metal nanoparticles are spatially separated in the solvent-free oxidation reaction. Apart from the BA oxidation for 0.5 and 1.0 h, the conversion and selectivity toward BZALD and toluene in BA oxidation for a longer reaction time of 6 h are summarized in Table S3. These reactivity trends over the series of Au and Pd catalysts are similar to those previously reported in the aqueous alcohol oxidation using Au and Pd metal nanoparticles as the catalysts supported on carbon (XC-72R), where OH^- serves as the oxidant for the ODH reaction.[1] Under aqueous conditions, it has been demonstrated that Pd operates as an electron scavenger through the oxygen reduction reaction ($O_2 + 2H_2O + 4e^- \rightarrow 4OH^-$).[1,2] However, in this work, such a reaction mechanism cannot be in operation; therefore, a modified reaction mechanism is proposed as the oxidation of BA proceeds in the absence of water, and molecular O_2 is used as the terminal oxidant.

The rate enhancement observed in the physical mixture of Au/CNT and Pd/CNT is further confirmed by first carrying out BA oxidation using one of the monometallic Pd/CNT or Au/CNT catalysts, followed by 1 h after the addition of the second monometallic catalyst. As shown in Figure 1b, the addition of Au/CNT to the reaction media over Pd/CNT increased the reaction rate from 0.87 to 1.4 $mM\cdot s^{-1}$, compared to the reaction using Pd/CNT in the absence of added Au/CNT. The same promotive effect is also observed when the order of catalyst mixing is reversed. In addition, we designed another experiment by performing BA oxidation using a fixed amount of Pd/CNT (50 mg) with the addition of increasing amounts of Au/CNT to the reaction mixture. The results presented in Figure 1c show that the conversion of BA increased linearly as the additional amount of Au/CNT increased; however, when a large amount of Au/CNT (100 mg) was added, the BA conversion decreased due to, possibly, mass transfer limitations. To exclude the influence of the blank reaction, we also carried out BA oxidation using bare CNTs with the same mass as that used for the catalytic experiments, where minimal conversions of 0.8 and 2.4% were observed at reaction times of 0.5 and 1 h, respectively (Figure 1d). This indicates that BA undergoes an autooxidation reaction, but this contribution is relatively minor compared to that observed over the metal-loaded catalysts. To confirm this, BA oxidation without any catalytic component was also conducted under the same reaction conditions, where similar conversions of 1.0% and 2.6% were observed at 0.5 and 1 h respectively (Figure S5). The above experiments demonstrate that Au/CNT + Pd/CNT exhibits a significant rate enhancement in the solvent-free oxidation of BA compared to that observed for the individual catalytic components.

High-resolution scanning transmission electron microscopy images (Figure 2a,b) show the characterization of the Au−Pd/

https://doi.org/10.1021/acscatal.4c05019
ACS Catal. 2024, 14, 16551−16561

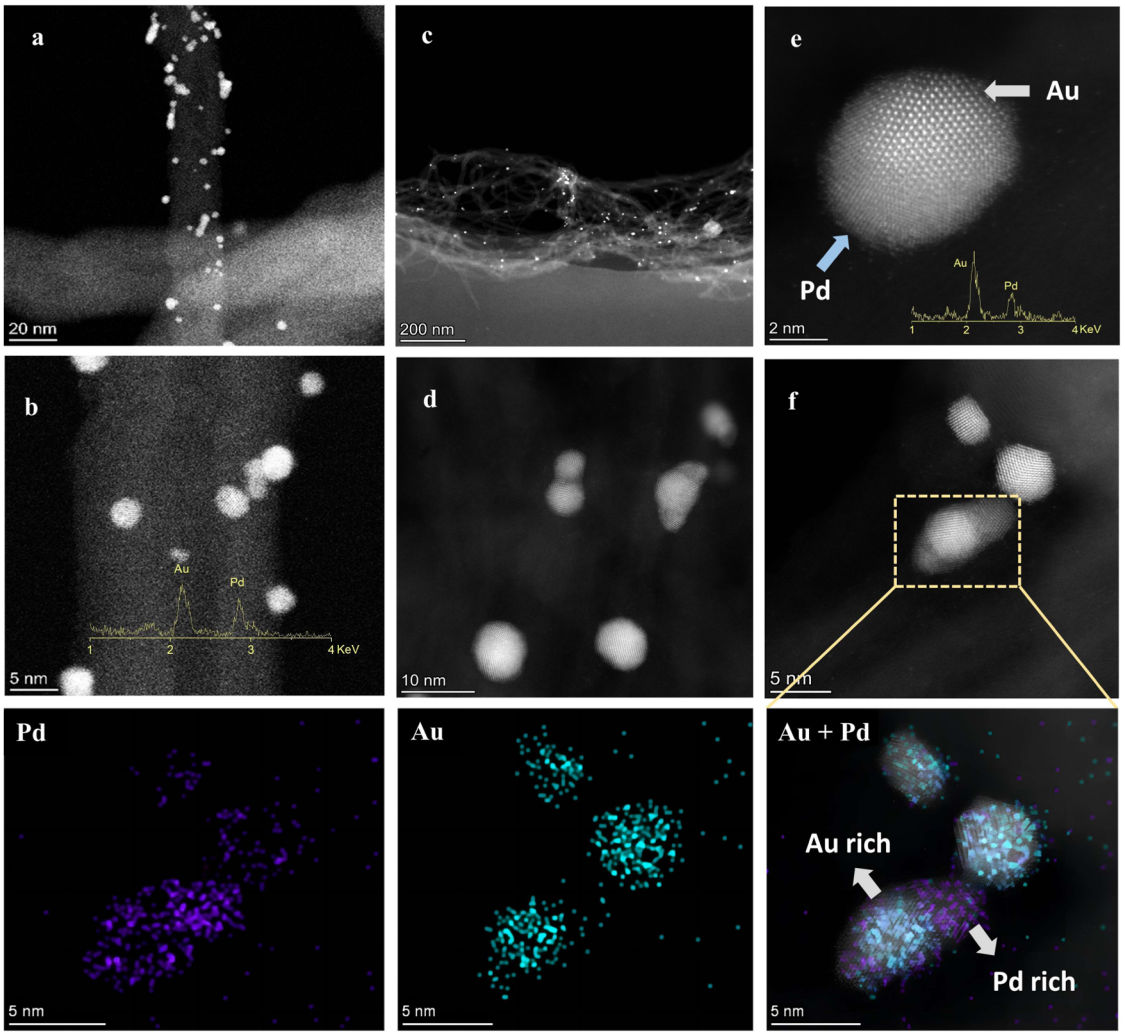

Figure 2. High-angle annular dark-field scanning transmission electron microscopy (HAADF-STEM) of Au−Pd/CNT (a, b) and the physical mixture of the Au/CNT + Pd/CNT catalysts after 0.5 h of reaction (c−f) with the corresponding elemental mapping images in (f). The arrows in e and f indicate that part of the monometallic nanoparticles tend to generate a Janus-like alloyed Au−Pd structure from the postreaction sample, where the two metal phases are affiliated with each other surfaces. The insets shown in (b and e) depict the EDS spectra of the corresponding particles, revealing peaks of Au M (about 2.1 keV) and Pd L (about 2.8 keV).

CNT alloy catalyst before the reaction and the physical mixture of Au/CNT + Pd/CNT after a reaction time of 0.5 h (Figure 2c−f). For the physical mixture, Au/CNT + Pd/CNT exhibited a high dispersion after the reaction (see Figure 2c), and we observed some migration of Pd, leading to small clusters of Pd situated on the surface of Au nanoparticles, forming a minority species of Janus-type nanoparticles, although inductively coupled plasma mass spectroscopy (ICP-MS) showed no leaching of either Au or Pd in the postreaction solution likely due to the sequestration of the physical mixture by the carbon. The Janus-type nanoparticles are shown in Figure 2e,f together with the corresponding elemental mapping characterization, showing that the nanoparticles comprise two metal phases (Au- and Pd-rich). This is also evidenced by a comparison with micrographs of the Au/CNT catalyst (Figure S4) and is distinctly different from the nanoparticles present in the alloyed Au−Pd/CNT catalyst (Figure 2b). The migration of Pd to Au could result from the high temperature (120 °C) and solvent-free reaction conditions and also dissolved O_2, which is known to promote either Ostwald ripening or particle agglomeration.[20] This result is consistent with the XPS characterization results for the Au/CNT + Pd/CNT physical mixture after the reaction, where the shift in binding energy indicates a stronger interaction between Au and Pd. Additional images are shown in Figure S6 to confirm this observation. To further investigate the transfer between Au and Pd nanoparticles, we characterized the physical mixture of Au/CNT and Pd/CNT after it was used in solvent-free BA oxidation under N_2, with all other reaction conditions remaining the same. As shown in Figure S7, when the reaction was carried out in an inert N_2 environment, the Au and Pd nanoparticles remained distinctly separated without forming alloyed or Janus-like particles. This suggests the critical role of O_2 during the selective oxidation of BA, as the higher likelihood of PdO formation and subsequent leaching due to the in situ formed water from DH and the reaction of Pd−H with O_2. This observation is consistent with the results shown in Figure S5b in the Supporting Information, where minor activity was observed when solvent-free BA oxidation was conducted under N_2.

We subsequently examined the stability of the Au/CNT + Pd/CNT catalysts when used as a physical mixture in solvent-

https://doi.org/10.1021/acscatal.4c05019
ACS Catal. 2024, 14, 16551−16561

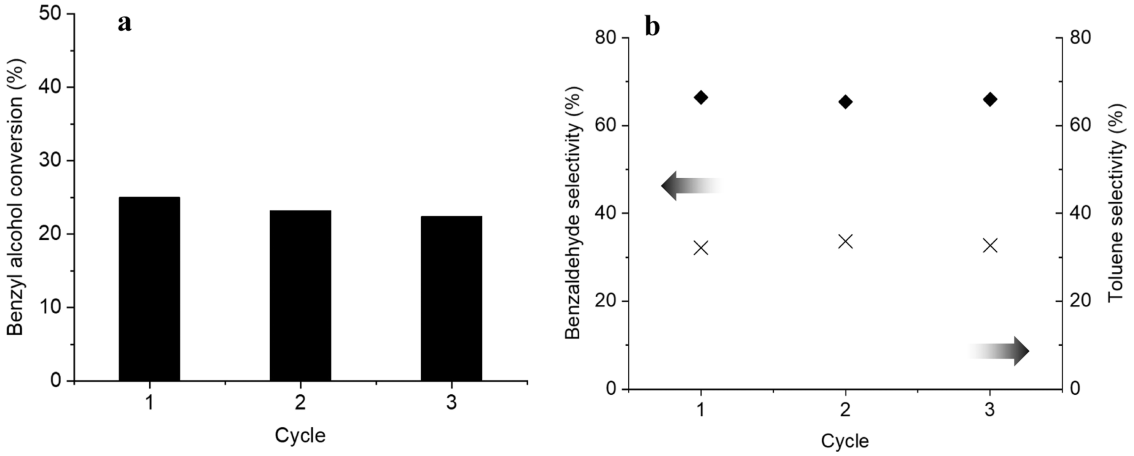

Figure 3. Solvent-free oxidation of BA over a physical mixture of Au/CNT + Pd/CNT for 3 cycles: (a) conversion and (b) product selectivity. *Reaction conditions*: 15 mL BA, 120 °C, 3 bar O_2, and reaction time of 0.5 h.

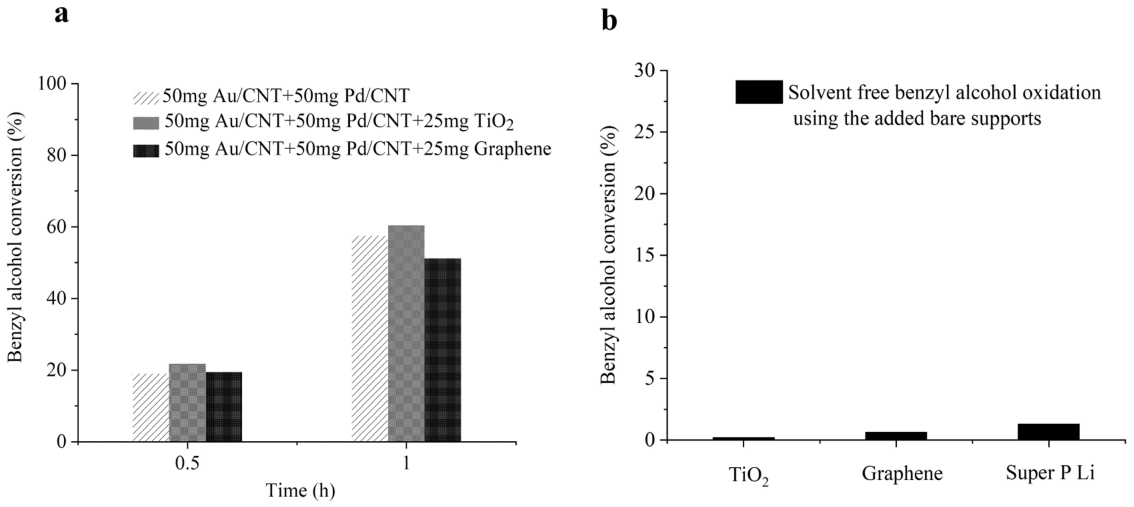

Figure 4. Solvent-free oxidation of BA over a physical mixture of Au/CNT + Pd/CNT as a catalyst with the addition of TiO_2 and graphene (a) and the corresponding blank reaction using different bare supports for 1 h reaction (b). *Reaction conditions*: 15 mL BA, 120 °C, and 3 bar O_2.

free BA oxidation. Figure 3 shows that the system is relatively stable for at least three reaction cycles with BA conversions of 25.0, 23.2, and 22.4% in each cycle (without changing the product selectivities). The decreased activity could be related to the migration of Pd to the Au nanoparticles during the reaction at 120 °C, where some Au−Pd Janus nanoparticles are observed after the reaction (Figures 2 and S6). Moreover, the catalytic activities observed for these Janus particles are still higher compared with those of the as-prepared Au−Pd alloy catalyst (BA conversion of 19.4% at 0.5 h). Furthermore, we tested the recyclability of the alloyed Au−Pd/CNT catalyst (Figure S8). Similarly, we observe a more severe decrease in activity in terms of BA conversion, where the number decreased by almost 30% compared to the first and third cycles. This indicates that, in addition to the alloying process, other factors, such as particle size distribution or leaching. may also affect the catalytic performance in solvent-free BA oxidation.

To distinguish the CORE effect in aqueous alcohol oxidation reactions from the rate enhancement observed in the solvent-free BA oxidation, we performed BA oxidation reactions using a physical mixture of Au/CNT + Pd/CNT with the addition of TiO_2 or graphene into the reaction mixture. The goal was to either retard or strengthen the electron transfer process during the reaction through the addition of a semiconductor (TiO_2 type p25) or an electron conductor (graphene) respectively (the conductivity among these support materials follows an order of CNTs > graphene ≫ TiO_2).[21,22] We have previously reported that electron transfer plays an important role in coupling the ODH of the alcohol and the oxygen reduction reaction (ORR). Figure 4a shows a similar conversion between the solvent-free oxidation of BA with or without the addition of TiO_2 and graphene, indicating that the electron transfer step is not the rate-determining step in solvent-free BA oxidation, while the added supports showed very minor activities on themselves as a blank reaction (Figure 4b). Therefore, it is likely that a different reaction mechanism is responsible for the observed rate enhancement effect in the present system.

BA oxidation is known to have two reaction pathways: namely BA dehydrogenation (DH) to BZALD and the parallel reaction of disproportionation with the product of toluene.[23] To understand the correlation between these two reaction routes, especially for the physical mixture catalyst, we have plotted the rates of disproportionation and DH over the monometallic Pd, and its combination with Au as an alloy and

https://doi.org/10.1021/acscatal.4c05019
ACS Catal. 2024, 14, 16551−16561

Table 1. Catalytic Performance of a Series of Carbon-Supported Au−Pd Catalysts in Solvent-Free BA Oxidation[a]

carbon-supported Au and Pd catalysts	conversion (%)	selectivity (%) BZALD		DH rate (mol·h^{-1}) TOL	Dis rate (mol·h^{-1})	DH/Dis ratio
Pd/CNT	8.6	78.6	13.4	0.0162	0.0033	4.9
Au−Pd/CNT	24.1	70.6	28.5	0.0292	0.0198	1.48
Au/CNTs + Pd/CNTs	29.4	68.3	30.5	0.0320	0.0259	1.24
Pd/XC-72	53.1	60.2	39.3	0.0342	0.0642	0.53
Au−Pd/XC-72	54.1	58.4	41.3	0.0285	0.0688	0.41
Au/XC-72 + Pd/XC-72	58.3	57.9	41.6	0.0292	0.0746	0.39
Au−Pd/Super P Li	31.89	79	20.7	0.0536	0.0190	2.82
Au/Super P Li + Pd/Super P Li	35.47	76.1	23.6	0.0537	0.0242	2.22

[a]Reaction conditions: 15 mL BA, 120 °C, 3 bar O_2, and 0.5 h. Note: the DH and Dis rates were calculated based on the given conversion and product selectivity.

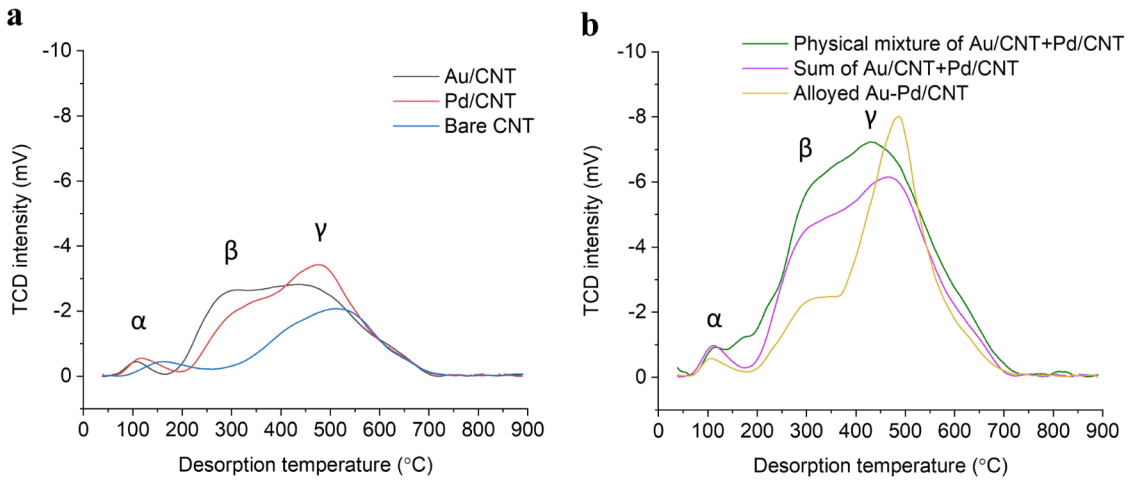

Figure 5. Hydrogen temperature-programmed desorption (H_2-TPD) profiles of (a) Au/CNT (25 mg), Pd/CNT(25 mg), and the bare CNT support (50 mg). (b) A physical mixture of Au/CNT + Pd/CNT (25 mg +25 mg) and the as-prepared alloyed Au−Pd/CNT (25 mg).

the physical mixture with different carbon supports (i.e., CNTs, XC-72R carbon black, and Super P Li (TIMCAL) with its blank reaction performed, as shown in Figure 4b). Interestingly, Table 1 shows that for all catalysts prepared on each of the carbon support materials, a physical mixture of monometallic catalysts exhibits a higher activity than the corresponding alloy catalyst. More interestingly, the physical mixture system is always more selective with respect to the reaction route of disproportionation (a lower rate of dehydrogenation/disproportionation, defined as DH/Dis in Table 1). Thus, a higher yield of toluene is obtained. It is worth noting that for the CNT-supported Au−Pd catalysts, whether the Pd is alloyed or physically mixed with Au as a bimetallic catalyst, the selectivity toward the disproportionation product can be greatly enhanced, especially for the physical mixture catalyst, where the disproportionation improved almost 3 times compared to the monometallic Pd catalyst; however, the monometallic Au catalyst did not show any activity. The activity trend toward the disproportionation direction follows the order Au/Pd physical mixture > Au−Pd alloy > Pd ≫ Au. That is to say, the addition of Au to the Pd catalyst during the reaction can drive the selectivity toward C−O bond activation in BA, resulting in higher productivity of the toluene product.[24,25] This is consistent with our previous studies, where we observed that the hydrogenolysis of the C−O bond in BA resulted from the presence of H on the Au surface, and this Au−H species facilitates toluene formation.[26,27] However, regarding the Au−Pd alloy, the electrochemical potential is a compromise between the two metals, indicating that although the disproportionation step can be improved in the alloy, the DH activity is usually limited. To confirm this, we examined the literature and some previous studies performed by our group. As summarized in Table 1, we found that most catalysts containing alloyed Au−Pd nanoparticles often show a high rate of the DH step to form BZALD, indicating a higher rate of DH/Dis. Furthermore, when we compare the same catalysts prepared on TiO_2 and carbon (see the rows with identical marked color in Table S4 in the supporting information), it normally shows a higher selectivity toward the reaction route of disproportionation, indicating that the carbon support facilitates the H species transfer during BA oxidation, which enhances the rate of disproportionation (Dis).[28,29] In our work, this phenomenon is more obvious for the physical mixture catalysts between Au/CNT and Pd/CNT. Here, the Pd−H species are formed via the DH pathway of benzyl alcohol and can react with O_2 to form benzaldehyde (BZALD) and H_2O. Meanwhile, owing to the strong collision between Au/CNT and Pd/CNT, a portion of the -H species on Pd partially transfers to the Au site via migration on the CNT and further reacts with benzyl alcohol to form toluene in the Dis pathway. We suggest that this additional pathway of H removal due to the transfer from Pd to Au results in an overall higher rate of benzyl alcohol consumption. Furthermore, we performed H_2-temperature-programmed desorption (TPD) studies to gain a deeper understanding of this process.

https://doi.org/10.1021/acscatal.4c05019
ACS Catal. 2024, 14, 16551−16561

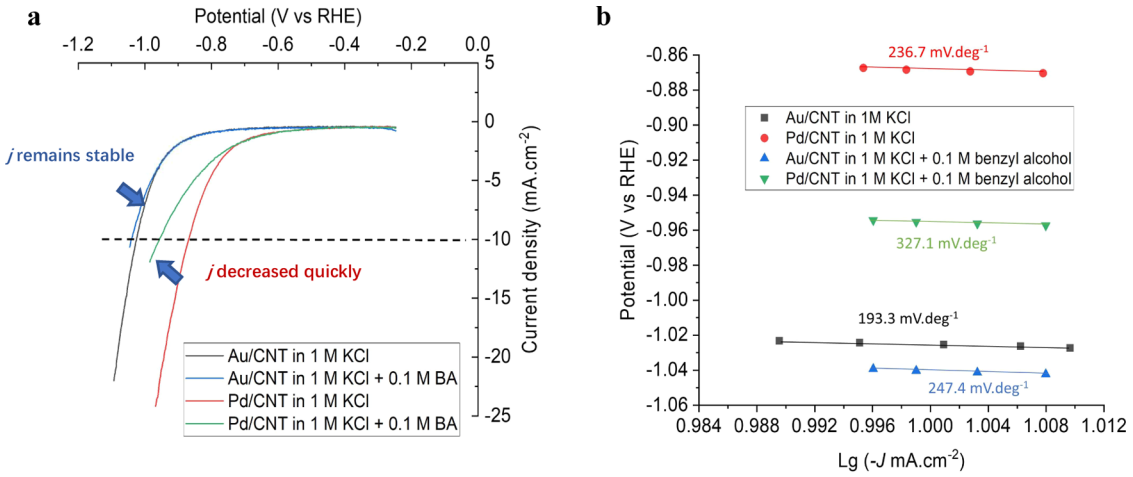

Figure 6. Electrochemical performance of linear sweep voltammetry (LSV) using Au/CNT and Pd/CNT in the hydrogen evolution reaction (HER) with or without benzyl alcohol (a) and the corresponding Tafel plots (b). Reaction conditions: the working electrode is the coated catalyst on a glassy carbon electrode, the counter electrode is the carbon rod, and 30 mL of 1 M KCl electrolyte in N_2, under stirring at a scan rate of 5 mV·s^{-1}.

Scheme 1. Proposed Reaction Route of Solvent-Free Oxidation of BA over the Pd Catalyst and its Combination with Au as a Physical Mixture Catalyst

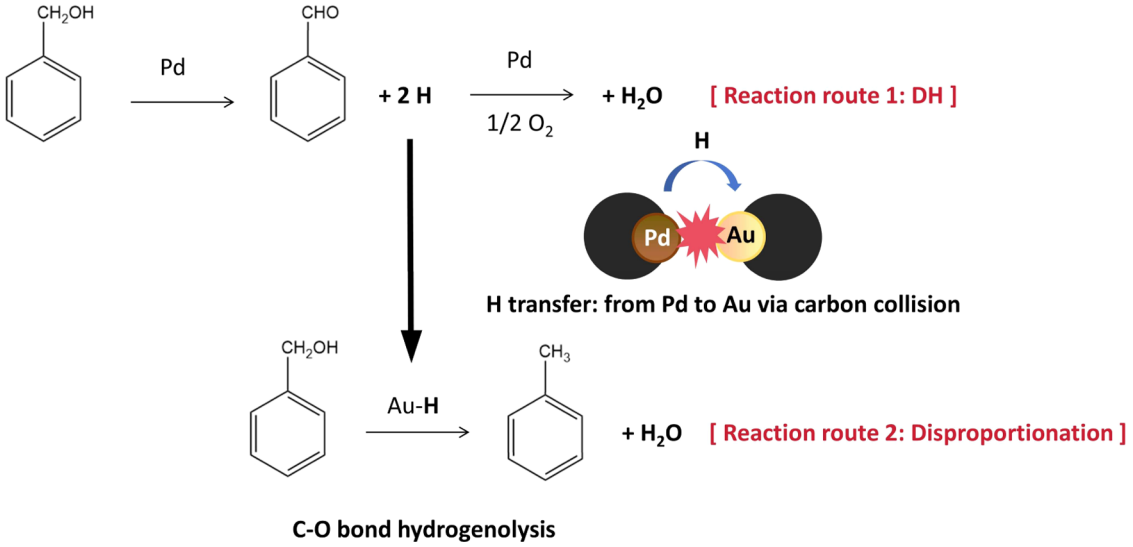

As shown in Figure 5, the H_2-TPD profiles of Au/CNT, Pd/CNT, bare CNT, and the physical mixture of Au/CNT and Pd/CNT were compared. The same mass (50 mg) of the samples was measured for all; in the case of the physical mixture system, 25 mg of each monometallic catalyst was mixed. To assign desorption peaks, the H_2-TPD profiles of monometallic catalysts and the bare support were analyzed first, displaying three major peaks, marked as α, β, and γ in Figure 5a. The α- and γ-peaks of bare CNTs can be assigned to the desorption of H species that are either weakly or strongly chemisorbed, respectively, with the latter signifying the C−H covalent bond formation.[30−33] The rate-determining step of H_2 desorption from the C−H bond in CNTs is assumed to be the association between two H species; meanwhile, H_2 desorption from an Au or Pd surface is much easier than from CNT.[32,34] Therefore, the β-peak, newly evolved in the samples containing metal nanoparticles at a temperature lower than that for the γ-peak, can be assigned to facilitate the desorption of H species by transfer from CNTs to the surface of metal nanoparticles. Notably, H_2 desorption on Au/CNT occurs at a lower temperature than that on Pd/CNT, implying that the activation energy for the transfer of H species from the CNTs to the Au surface is smaller than that from the CNTs to the Pd surface. This supports our hypothesis that H species can transfer from the Pd surface to the Au surface through CNTs because of the strong collision between catalyst particles in our slurry-like system, resulting from the addition of a large amount of carbon-based catalyst (100 mg) to 15 mL of BA substrate (Figure S9). In this case, the CNT surface is most likely to act as a carrier material, providing an environment for the migration of −H species and the interaction between Au and Pd.[28,35] Next, to confirm if additional H_2 desorption routes are generated by physically mixing Au/CNT and Pd/CNT, the desorption curve of the physical mixture was compared with the sum of the desorption curves of the two monometallic catalysts, as shown in Figure 5b. The two curves should be analogous to each other if Au/CNT and Pd/CNT are independent, without any interaction between them. In

https://doi.org/10.1021/acscatal.4c05019
ACS Catal. 2024, 14, 16551−16561

contrast, the β- and γ-peaks of the physical mixture are larger than the sum of the desorption curves. This may imply that additional H_2 was dissociatively adsorbed to the surface of a Pd nanoparticle and then transferred to Au/CNT physically contacting the Pd/CNT, given that H_2 dissociative adsorption is more facile on the Pd surface than on the Au surface and carbon materials.[34,36] Furthermore, the β-peak of the alloyed Au−Pd/CNT catalyst showed even smaller desorption of H_2, which was likely to have an alloyed structure whose surface was rich in Au; hence, this catalyst was unable to adsorb a large amount of H_2.[37] When the desorption procedure begins, these additional H species may finally be desorbed from Au/CNT.

To provide further evidence of this, we have also tried to understand the interaction between Au−H and Pd−H electrochemically by observing the electrochemical hydrogen evolution reaction (HER) using Au/CNT and Pd/CNT, respectively, with or without the presence of BA. Figure 6 shows that Pd/CNT exhibits higher activity in the HER (∼0.2 V potential gap at a current density of 10 mA.cm^{-2}) than Au/CNT in an electrolyte without the addition of BA, suggesting that the Pd surface is a good catalytic site to interact with the surface H species dehydrogenated from BA.[38] However, once BA was added to the electrolyte, the HER activity over Pd/CNT decreased quickly, whereas Au/CNT remained quite stable. This indicates that the Pd surface is largely affected by the competitive adsorption between the surface H, H_2O, and BA, whereas Au is relatively inert to these species.[39] Comparatively, in terms of the thermochemical DH of BA, it is recognized that the binding energy of surface H on Au is weak, and hence these surface H species can more easily react with BA, leading to the C−O bond hydrogenolysis to form toluene instead of reducing O_2 to H_2O, the final step of DH process in light of a negligible activity of O_2 dissociation on pure gold.[40] We, therefore, propose the reaction route preference in solvent-free oxidation of BA over the Pd catalyst and its combination with Au as a physical mixture catalyst, as shown in Scheme 1. Here, we consider that the addition of Au strengthens the coupling effect between the DH and disproportionation processes in the solvent-free oxidation of BA via surface H spillover from Pd to Au. Transferring the surface H species from Pd to Au enables dissociation of the C−O bond, which is known to be more challenging than the C−H bond activation.[41−43]

CONCLUSIONS

The rate enhancement observed in solvent-free BA oxidation when using a physical mixture of Au/CNT and Pd/CNT can be ascribed to the coupling of the BA DH and disproportionation reactions. This is different from the origin of the rate enhancement observed in an aqueous base, which is the coupling of the ODH and ORR reactions responsible for the observed CORE effect. However, it is clear that coupling the two processes can lead to significant rate enhancement if the two metallic sites responsible for the two separate processes can be spatially separated. Furthermore, we consider that the observation of effective coupling between BA DH and disproportionation can provide new insights into the design of multicomponent heterogeneous catalysts.

METHODS

Chemicals. The chemical reagents, including BA, BZALD, BZA, and toluene used in the experiments, were purchased from Aladdin Company (China) and used without further purification: BA (99.8%, purity); multiwalled carbon nanotubes (CNTs) (99% purity; Chendu Organic Chemicals); Super P Li carbon black (TIMCAL Super P Conductive Carbon Black has numerous battery applications as a conductive additive; Shenzhen Tianchenghe Technology Co., Ltd., Shenzhen, China); $PdCl_2$ (99.999% metal basis); $NaBH_4$ (98%, metal basis); $HAuCl_4{\cdot}3H_2O$ (≥99.9% trace metal basis); poly(vinyl alcohol) (Sigma-Aldrich, Mw 9000−10,000, 80% hydrolyzed); sulfuric acid (H_2SO_4; Fisher Scientific, ≥95%); deionized water (DI water, Millipore; 18.2 MΩ·cm at 25 °C); Carbon Vulcan XC-72R (Cabot Corporation); titanium dioxide (TiO_2, Degussa P25); O_2 (99.999% purity; Taiyuan Iron and Steel Corporation). All used electrodes were supplied by Gaossunion Photoelectric Technology.

Material Preparation. *Synthesis of 0.5 wt % Au/CNT and 0.5 wt % Pd/CNT Catalysts by Sol Immobilization.* 1.0 mL of $HAuCl_4$ solution (5 mg Au/mL) or 1.0 mL of $PdCl_2$ solution (5 mg Pd/mL) were added to 300 mL of deionized (DI) water and the mixed solution was stirred at room temperature for 15 min. The PVA solution was subsequently added at a mass ratio of PVA to Au or Pd of 1:1. Then, the required amount of freshly prepared $NaBH_4$ solution at a molar ratio of $NaBH_4$ to Au or Pd of 5:1 was added to the above-mixed solution to form a dark red or brown solution, respectively. After stirring for 30 min, 0.995 g of CNT was added, and the pH of the mixed solution was adjusted to 1 with H_2SO_4. After 1 h, the products were filtered, washed with deionized water, and dried at 110 °C for 18 h in an oven.

Synthesis of the Alloyed 1.0 wt % Au−Pd/CNT Catalyst by Sol Immobilization. The steps for the synthesis of the 1 wt % Au−Pd/CNT catalyst were similar to the above procedure. 5 mg of Au and 5 mg of the Pd precursor were added at the same time to the solution, and the weight of the CNT was changed from 0.995 to 0.99 g.

Synthesis of 1.0 wt % Au/XC-72 and 1.0 wt % Pd/XC-72 Catalysts by Sol Immobilization. The XC-72R-supported monometallic Au and Pd catalysts were prepared using a method similar to the above procedure. Typically, 0.909 mL of the $HAuCl_4$ precursor solution (11 mg/mL) or 1.0 mL of the $PdCl_2$ precursor solution (10 mg/mL) was added to 140 mL of DI water at room temperature. The required amount of PVA (PVA/metal = 1/1 (w/w)) was added to the above solution, followed by the addition of $NaBH_4$ leading to the sudden color changes to dark red or brown, indicating the formation of Au or Pd colloid. After 30 min of stirring, 0.99 g of XC-72R carbon was added and the slurry was further stirred for another 30 min. The catalysts are denoted as Au/XC-72 and Pd/XC-72. The resulting catalyst was washed with 1 L DI water, filtered, and dried at 110 °C for 16 h.

Synthesis of 1 wt % Au/Super P Li and 1 wt % Pd/Super P Li catalysts by Sol Immobilization. The Super P Li carbon black-supported monometallic Au and Pd catalysts were prepared using a methodology similar to that described above. The only difference is the use of Super P Li as the support.

Benzyl Alcohol Oxidation. *Testing of Catalysts in Solvent-Free BA Oxidation Reaction.* Solvent-free aerobic oxidation of BA using the molecular oxidant O_2 was conducted in a glass reactor (50 mL) fitted with a magnetic stirrer. First, the glass reactor was charged with benzyl alcohol (15 mL) and the catalyst (50 mg, for example, 50 mg 0.5% Au/CNT + 50 mg 0.5% Pd/CNT as a physical mixture; 50 mg monometallic

https://doi.org/10.1021/acscatal.4c05019
ACS Catal. 2024, 14, 16551−16561

0.5% Pd/CNT; 50 mg monometallic 0.5% Au/CNT; and 50 mg alloyed 1.0% Au−Pd/CNT) before it was purged five times with oxygen. Subsequently, the reactor was pressurized to 0.3 MPa with O_2 at 25 °C. The reaction mixture was heated to the required temperature at 1000 rpm. The reactor was also connected to an oxygen reservoir for the purpose of replenishing the oxygen consumed during the reaction. The reaction products were analyzed by GC (FuLi GC9790, China) equipped with a flame ionization detector (FID) and DM-5 column (30 m × 0.25 mm × 0.25 lm). The electrochemical reaction of hydrogen evolution was conducted in a single-cell reactor using a potentiostat (ChenHua, CHI760E). The working electrode was prepared by dispersing 5 mg of the catalyst into 1 mL (900 μL H_2O + 100 μL Nafion) solution under sonication for 5 min, followed by dropping 5 μL solution onto a glassy carbon electrode (with a diameter of 3 mm) and drying under atmospheric conditions. A carbon rod was used as the counter electrode, and a saturated calomel electrode (SCE) was used as the reference electrode. The reaction was performed under N_2, and the obtained potential numbers were converted using a reversible hydrogen electrode (RHE) via E(RHE) = E(SCE) + 0.0591 pH + 0.24.

Catalyst Characterization. Atomic-resolution HAADF-STEM images and EDX mappings were collected by an FEI Titan Cubed Themis G2 300 (Thermo Fischer Scientific) and JEM-ARM300F2. Inductively coupled plasma-atomic emission spectroscopy was measured at the spectral range ranging from 167 to 782 nm (242.79 nm for Au and 340.46 nm for Pd) using an argon plasma source on an OPTIMA 8300 (PerkinElmer) with a detection limit of 10 ppb. X-ray photoelectron spectra (XPS) were collected using a Kratos AXIS ULTRA DLD system (Shimadzu, Japan) with an Al Ka source (1486.6 eV), and the C1 s peak at 284.8 eV was used as a reference for calibration. An ASAP2020 instrument (Micromeritics) was used to analyze the BET surface area, pore diameter, and pore volume of the prepared samples. BET and t-plot methods were used to obtain the specific area and micropore volume. H_2-TPD was performed according to the following program: step 1: 50 mg catalyst was dried under Ar for 1 h at 120 °C; step 2: cooling the temperature down to room temperature and switching the gas to H_2 (20 mL.min^{-1}) for 1 h; step 3: switching back to Ar for a further 15 min before recording the TPD signal, the system was set to 900 °C with a ramp of 20 °C.min^{-1}.

■ ASSOCIATED CONTENT

Data Availability Statement

All data needed to evaluate the conclusions in the paper are present in the paper or the Supporting Information.

Supporting Information

The Supporting Information is available free of charge at https://pubs.acs.org/doi/10.1021/acscatal.4c05019.

BET surface area, XPS spectra, catalytic performance data in solvent-free BA oxidation, HRTEM images with elemental analysis and particle size distribution over the series of Au and Pd catalysts (PDF)

■ AUTHOR INFORMATION

Corresponding Authors

Mark Douthwaite − *Max Planck-Cardiff Centre on the Fundamentals of Heterogeneous Catalysis FUNCAT, Cardiff Catalysis Institute, School of Chemistry, Cardiff University, Translational Research Hub, Cardiff University, Cardiff CF24 4HQ, U.K.*; Email: douthwaitejm@cardiff.ac.uk

Xiaoyang Jerry Huang − *Max Planck-Cardiff Centre on the Fundamentals of Heterogeneous Catalysis FUNCAT, Cardiff Catalysis Institute, School of Chemistry, Cardiff University, Translational Research Hub, Cardiff University, Cardiff CF24 4HQ, U.K.; Center of Advanced Electrochemical Energy, Institute of Advanced Interdisciplinary Studies, Chongqing University, Chongqing 400044, China*; orcid.org/0000-0002-7221-2075; Email: huang_xy@cqu.edu.cn

Graham J. Hutchings − *Max Planck-Cardiff Centre on the Fundamentals of Heterogeneous Catalysis FUNCAT, Cardiff Catalysis Institute, School of Chemistry, Cardiff University, Translational Research Hub, Cardiff University, Cardiff CF24 4HQ, U.K.*; orcid.org/0000-0001-8885-1560; Email: hutch@cardiff.ac.uk

Authors

Xiaoliang Li − *State Key Laboratory of Clean and Efficient Coal Utilization, College of Chemistry and Chemical Engineering, Taiyuan University of Technology, Taiyuan 030024 Shanxi, China*

Liang Zhao − *Max Planck-Cardiff Centre on the Fundamentals of Heterogeneous Catalysis FUNCAT, Cardiff Catalysis Institute, School of Chemistry, Cardiff University, Translational Research Hub, Cardiff University, Cardiff CF24 4HQ, U.K.; BASF Advanced Chemicals Co., Ltd., Shanghai 200137, China*; orcid.org/0000-0002-4956-9447

Kai Wang − *Max Planck-Cardiff Centre on the Fundamentals of Heterogeneous Catalysis FUNCAT, Cardiff Catalysis Institute, School of Chemistry, Cardiff University, Translational Research Hub, Cardiff University, Cardiff CF24 4HQ, U.K.*; orcid.org/0000-0002-1918-4781

Ouardia Akdim − *Max Planck-Cardiff Centre on the Fundamentals of Heterogeneous Catalysis FUNCAT, Cardiff Catalysis Institute, School of Chemistry, Cardiff University, Translational Research Hub, Cardiff University, Cardiff CF24 4HQ, U.K.*; orcid.org/0000-0003-3915-7681

Isaac T. Daniel − *Max Planck-Cardiff Centre on the Fundamentals of Heterogeneous Catalysis FUNCAT, Cardiff Catalysis Institute, School of Chemistry, Cardiff University, Translational Research Hub, Cardiff University, Cardiff CF24 4HQ, U.K.*

Rena Oh − *School of Energy and Power Engineering, Chongqing University, Chongqing 400044, China*

Lei Liu − *State Key Laboratory of Clean and Efficient Coal Utilization, College of Chemistry and Chemical Engineering, Taiyuan University of Technology, Taiyuan 030024 Shanxi, China*; orcid.org/0000-0003-2027-4271

Zhe Wang − *State Key Laboratory of Clean and Efficient Coal Utilization, College of Chemistry and Chemical Engineering, Taiyuan University of Technology, Taiyuan 030024 Shanxi, China*

Fanhui Meng − *State Key Laboratory of Clean and Efficient Coal Utilization, College of Chemistry and Chemical Engineering, Taiyuan University of Technology, Taiyuan 030024 Shanxi, China*; orcid.org/0000-0003-0998-5179

Samuel Pattisson − *Max Planck-Cardiff Centre on the Fundamentals of Heterogeneous Catalysis FUNCAT, Cardiff Catalysis Institute, School of Chemistry, Cardiff University,*

https://doi.org/10.1021/acscatal.4c05019
ACS Catal. 2024, 14, 16551−16561

Translational Research Hub, Cardiff University, Cardiff CF24 4HQ, U.K.

Angeles López-Martin − *Max Planck-Cardiff Centre on the Fundamentals of Heterogeneous Catalysis FUNCAT, Cardiff Catalysis Institute, School of Chemistry, Cardiff University, Translational Research Hub, Cardiff University, Cardiff CF24 4HQ, U.K.*

Jian Yang − *Center of Advanced Electrochemical Energy, Institute of Advanced Interdisciplinary Studies, Chongqing University, Chongqing 400044, China*

Richard J. Lewis − *Max Planck-Cardiff Centre on the Fundamentals of Heterogeneous Catalysis FUNCAT, Cardiff Catalysis Institute, School of Chemistry, Cardiff University, Translational Research Hub, Cardiff University, Cardiff CF24 4HQ, U.K.;* orcid.org/0000-0001-9990-7064

Complete contact information is available at: https://pubs.acs.org/10.1021/acscatal.4c05019

Author Contributions

X.L., X.J.H., and M.D. contributed to the design of the study; X.L., Z.W., L.Z., R.O., and K.W. conducted experiments and data analysis. M.D., X.J.H., and G.J.H. conceived the mechanism study; X.J.H., M.D., L.Z., and G.J.H. wrote the manuscript. All authors discussed and contributed to the work.

Notes

The authors declare no competing financial interest.

■ ACKNOWLEDGMENTS

X.L. acknowledges the Natural Science Basic Research Plan in Shanxi Province of China (No.20210302123093). K.W. and L.Z. thank the China Scholarship Council for PhD funding. X.J.H. and J.Y. appreciate the technical support from the S.G.S. group at Xiamen University. The authors acknowledge the assistance of Instrumental Analysis Center Taiyuan University of Technology (TEM Model Name: JEM-ARM300F2).

■ REFERENCES

(1) Huang, X.; Akdim, O.; Douthwaite, M.; Wang, K.; Zhao, L.; Lewis, R. J.; Pattisson, S.; Daniel, I. T.; Miedziak, P. J.; Shaw, G.; Morgan, D. J.; Althahban, S. M.; Davies, T. E.; He, Q.; Wang, F.; Fu, J.; Bethell, D.; McIntosh, S.; Kiely, C. J.; Hutchings, G. J. Au−Pd Separation Enhances Bimetallic Catalysis of Alcohol Oxidation. *Nature* **2022**, *603* (7900), 271−275.

(2) Zhao, L.; Akdim, O.; Huang, X.; Wang, K.; Douthwaite, M.; Pattisson, S.; Lewis, R. J.; Lin, R.; Yao, B.; Morgan, D. J.; Shaw, G.; He, Q.; Bethell, D.; McIntosh, S.; Kiely, C. J.; Hutchings, G. J. Insights into the Effect of Metal Ratio on Cooperative Redox Enhancement Effects over Au- and Pd-Mediated Alcohol Oxidation. *ACS Catal.* **2023**, *13* (5), 2892−2903.

(3) Daniel, I. T.; Kim, B.; Douthwaite, M.; Pattisson, S.; Lewis, R. J.; Cline, J.; Morgan, D. J.; Bethell, D.; Kiely, C. J.; McIntosh, S.; Hutchings, G. J. Electrochemical Polarization of Disparate Catalytic Sites Drives Thermochemical Rate Enhancement. *ACS Catal.* **2023**, *13* (21), 14189−14198.

(4) Kim, B.; Daniel, I.; Douthwaite, M.; Pattisson, S.; Hutchings, G. J.; McIntosh, S. Tafel Analysis Predicts Cooperative Redox Enhancement Effects in Thermocatalytic Alcohol Dehydrogenation. *ACS Catal.* **2024**, *14*, 8488−8493.

(5) Daniel, I. T.; Zhao, L.; Bethell, D.; Douthwaite, M.; Pattisson, S.; Lewis, R. J.; Akdim, O.; Morgan, D. J.; McIntosh, S.; Hutchings, G. J. Kinetic Analysis to Describe Co-Operative Redox Enhancement Effects Exhibited by Bimetallic Au–Pd Systems in Aerobic Oxidation. *Catal. Sci. Technol.* **2023**, *13* (1), 47−55.

(6) Zope, B. N.; Hibbitts, D. D.; Neurock, M.; Davis, R. J. Reactivity of the gold/water Interface During Selective Oxidation Catalysis. *Science* **2010**, *330*, 74−79.

(7) Ryu, J.; Bregante, D. T.; Howland, W. C.; Bisbey, R. P.; Kaminsky, C. J.; Surendranath, Y. Thermochemical Aerobic Oxidation Catalysis in Water Can Be Analysed as Two Coupled Electrochemical Half-Reactions. *Nat. Catal.* **2021**, *4* (9), 742−752.

(8) Lodaya, K. M.; Tang, B. Y.; Bisbey, R. P.; Weng, S.; Westendorff, K. S.; Toh, W. L.; Ryu, J.; Román-Leshkov, Y.; Surendranath, Y. An Electrochemical Approach for Designing Thermochemical Bimetallic Nitrate Hydrogenation Catalysts. *Nat. Catal.* **2024**, *7* (3), 262−272.

(9) Miyake, T.; Rolandi, M. Grotthuss Mechanisms: From Proton Transport in Proton Wires to Bioprotonic Devices. *J. Phys.: Condens. Matter* **2015**, *28* (2), 23001.

(10) Enache, D. I.; Edwards, J. K.; Landon, P.; Solsona-Espriu, B.; Carley, A. F.; Herzing, A. A.; Watanabe, M.; Kiely, C. J.; Knight, D. W.; Hutchings, G. J. Solvent-Free Oxidation of Primary Alcohols to Aldehydes Using Au-Pd/TiO_2 Catalyst. *Science* **2006**, *311* (5759), 362−365.

(11) Chan-Thaw, C. E.; Savara, A.; Villa, A. Selective Benzyl Alcohol Oxidation over Pd Catalysts. *Catalysts* **2018**, *8* (10), No. 431.

(12) Miedziak, P.; Sankar, M.; Dimitratos, N.; Lopez-Sanchez, J. A.; Carley, A. F.; Knight, D. W.; Taylor, S. H.; Kiely, C. J.; Hutchings, G. J. Oxidation of Benzyl Alcohol Using Supported Gold–Palladium Nanoparticles. *Catal. Today* **2011**, *164* (1), 315−319.

(13) Lewis, R. J.; Hutchings, G. J. Selective Oxidation Using In Situ-Generated Hydrogen Peroxide. *Acc. Chem. Res.* **2024**, *57* (1), 106−119.

(14) Li, J.; Zhao, S.; Zhang, L.; Jiang, S. P.; Yang, S.-Z.; Wang, S.; Sun, H.; Johannessen, B.; Liu, S. Cobalt Single Atoms Embedded in Nitrogen-Doped Graphene for Selective Oxidation of Benzyl Alcohol by Activated Peroxymonosulfate. *Small* **2021**, *17* (16), No. 2004579.

(15) Sankar, M.; Nowicka, E.; Carter, E.; Murphy, D. M.; Hutchings, G. J.; et al. The Benzaldehyde Oxidation Paradox Explained by the Interception of Peroxy Radical by Benzyl Alcohol. *Nat. Commun.* **2014**, *5* (1), No. 3332.

(16) Hutchings, G. J. Selective Oxidation Using Supported Gold Bimetallic and Trimetallic Nanoparticles. *Catal. Today* **2014**, *238*, 69−73.

(17) Cao, E.; Sankar, M.; Nowicka, E.; He, Q.; Morad, M.; Miedziak, P. J.; Taylor, S. H.; Knight, D. W.; Bethell, D.; Kiely, C. J.; et al. Selective Suppression of Disproportionation Reaction in Solvent-Less Benzyl Alcohol Oxidation Catalysed by Supported Au-Pd Nanoparticles. *Catal. today* **2013**, *203*, 146−152.

(18) Davis, S. E.; Ide, M. S.; Davis, R. J. Selective Oxidation of Alcohols and Aldehydes over Supported Metal Nanoparticles. *Green Chem.* **2013**, *15*, 17−45.

(19) Douthwaite, M.; Huang, X.; Iqbal, S.; Miedziak, P. J.; Brett, G. L.; Kondrat, S. A.; Edwards, J. K.; Sankar, M.; Knight, D. W.; Bethell, D.; Hutchings, G. J. The Controlled Catalytic Oxidation of Furfural to Furoic Acid Using AuPd/$Mg(OH)_2$. *Catal. Sci. Technol.* **2017**, *7* (22), 5284−5293.

(20) Hansen, T. W.; Delariva, A. T.; Challa, S. R.; Datye, A. K. Sintering of Catalytic Nanoparticles: Particle Migration or Ostwald Ripening? *Acc. Chem. Res.* **2013**, *46* (8), 1720−1730.

(21) Othman, M. A.; Amat, N. F.; Ahmad, B. H.; Rajan, J. Electrical Conductivity Characteristic of TiO_2 Nanowires from Hydrothermal Method. *J. Phys.: Conf. Ser.* **2014**, *495*, No. 12027.

(22) Marinho, B.; Ghislandi, M.; Tkalya, E.; Koning, C. E.; de With, G. Electrical Conductivity of Compacts of Graphene, Multi-Wall Carbon Nanotubes, Carbon Black, and Graphite Powder. *Powder Technol.* **2012**, *221*, 351−358.

(23) Galvanin, F.; Sankar, M.; Cattaneo, S.; Bethell, D.; Dua, V.; Hutchings, G. J.; Gavriilidis, A. On the Development of Kinetic Models for Solvent-Free Benzyl Alcohol Oxidation over a Gold-Palladium Catalyst. *Chem. Eng. J.* **2018**, *342*, 196−210.

(24) Abad, A.; Concepción, P.; Corma, A.; Garcia, H. A Collaborative Effect between Gold and a Support Induces the

Selective Oxidation of Alcohols. *Angew. Chem., Int. Ed.* **2005**, *44* (26), 4066−4069.
(25) Abad, A.; Almela, C.; Corma, A.; Garcia, H. Unique Gold Chemoselectivity for the Aerobic Oxidation of Allylic Alcohols. *Chem. Commun.* **2006**, *30*, 3178−3180.
(26) Lopez-Sanchez, J. A.; Dimitratos, N.; Glanville, N.; Kesavan, L.; Hammond, C.; Edwards, J. K.; Carley, A. F.; Kiely, C. J.; Hutchings, G. J. Reactivity Studies of Au-Pd Supported Nanoparticles for Catalytic Applications. *Appl. Catal. A Gen.* **2011**, *391* (1−2), 400−406.
(27) Dimitratos, N.; Lopez-Sanchez, J. A.; Morgan, D.; Carley, A.; Prati, L.; Hutchings, G. J. Solvent Free Liquid Phase Oxidation of Benzyl Alcohol Using Au Supported Catalysts Prepared Using a Sol Immobilization Technique. *Catal. today* **2007**, *122* (3−4), 317−324.
(28) Navarro-Ruiz, J.; Audevard, J.; Vidal, M.; Campos, C. H.; Del Rosal, I.; Serp, P.; Gerber, I. C. Mechanism of Hydrogen Spillover on Metal-Doped Carbon Materials: Surface Carboxylic Groups Are Key. *ACS Catal.* **2024**, *14* (9), 7111−7126.
(29) Sha, X.; Knippenberg, M. T.; Cooper, A. C.; Pez, G. P.; Cheng, H. Dynamics of Hydrogen Spillover on Carbon-Based Materials. *J. Phys. Chem. C* **2008**, *112* (44), 17465−17470.
(30) Ioannatos, G. E.; Verykios, X. E. H_2 Storage on Single- and Multi-Walled Carbon Nanotubes. *Int. J. Hydrogen Energy* **2010**, *35*, 622−628.
(31) Züttel, A.; Nützenadel, C.; Sudan, P.; Mauron, P.; Emmenegger, C.; Rentsch, S.; Schlapbach, L.; Weidenkaff, A.; Kiyobayashi, T. Hydrogen Sorption by Carbon Nanotubes and Other Carbon Nanostructures. *J. Alloys Compd.* **2002**, *330*−*332*, 676−682.
(32) Ishii, T.; Ozaki, J. Estimation of the Spatial Distribution of Carbon Edge Sites in a Carbon Structure Using H_2 Desorption Kinetics in Temperature Programmed Desorption. *Carbon* **2022**, *196*, 1054−1062.
(33) Yamanaka, S.; Fujikane, M.; Uno, M.; Murakami, H.; Miura, O. Hydrogen Content and Desorption of Carbon Nano-Structures. *J. Alloys Compd.* **2004**, *366* (1−2), 264−268.
(34) Lucci, F. R.; Darby, M. T.; Mattera, M. F. G.; Ivimey, C. J.; Therrien, A. J.; Michaelides, A.; Stamatakis, M.; Sykes, E. C. H. Controlling Hydrogen Activation, Spillover, and Desorption with Pd-Au Single-Atom Alloys. *J. Phys. Chem. Lett.* **2016**, *7* (3), 480−485.
(35) Geng, Y.; Li, H. Hydrogen Spillover-Enhanced Heterogeneously Catalyzed Hydrodeoxygenation for Biomass Upgrading. *ChemSusChem* **2022**, *15* (8), No. e202102495.
(36) Zlotea, C.; Cuevas, F.; Paul-Boncour, V.; Leroy, E.; Dibandjo, P.; Gadiou, R.; Vix-Guterl, C.; Latroche, M. Size Dependent Hydrogen Sorption in Ultrasmall Pd Clusters Embedded in a Mesoporous Carbon Template. *J. Am. Chem. Soc.* **2010**, *132* (22), 7720−7729.
(37) Liu, R.; Yu, Y.; Yoshida, K.; Li, G.; Jiang, H.; Zhang, M.; Zhao, F.; Fujita, S. ichiro.; Arai, M. Physically and Chemically Mixed TiO_2-Supported Pd and Au Catalysts: Unexpected Synergistic Effects on Selective Hydrogenation of Citral in Supercritical CO_2. *J. Catal.* **2010**, *269*, 191−200.
(38) Zhang, L.; Chang, Q.; Chen, H.; Shao, M. Recent Advances in Palladium-Based Electrocatalysts for Fuel Cell Reactions and Hydrogen Evolution Reaction. *Nano Energy* **2016**, *29*, 198−219.
(39) Heinz, H.; Farmer, B. L.; Pandey, R. B.; Slocik, J. M.; Patnaik, S. S.; Pachter, R.; Naik, R. R. Nature of Molecular Interactions of Peptides with Gold, Palladium, and Pd- Au Bimetal Surfaces in Aqueous Solution. *J. Am. Chem. Soc.* **2009**, *131* (28), 9704−9714.
(40) Sault, A. G.; Madix, R. J.; Campbell, C. T. Adsorption of Oxygen and Hydrogen on Au (110)-(1 × 2). *Surf. Sci.* **1986**, *169* (2−3), 347−356.
(41) Conte, M.; Miyamura, H.; Kobayashi, S.; Chechik, V. Spin Trapping of Au-H Intermediate in the Alcohol Oxidation by Supported and Unsupported Gold Catalysts. *J. Am. Chem. Soc.* **2009**, *131* (20), 7189−7196.
(42) Balcells, D.; Clot, E.; Eisenstein, O. C-H Bond Activation in Transition Metal Species from a Computational Perspective. *Chem. Rev.* **2010**, *110* (2), 749−823.
(43) Goulas, K. A.; Mironenko, A. V.; Jenness, G. R.; Mazal, T.; Vlachos, D. G. Fundamentals of C-O Bond Activation on Metal Oxide Catalysts. *Nat. Catal.* **2019**, *2* (3), 269−276.

https://doi.org/10.1021/acscatal.4c05019
ACS Catal. 2024, 14, 16551−16561